Bioactive Materials 25 (2023) 1–12

Contents lists available at ScienceDirect

Bioactive Materials

journal homepage: www.keaipublishing.com/en/journals/bioactive-materials

Infection-responsive long-term antibacterial bone plates for open fracture therapy

Lujiao Zhang [a], Yurun Yang [b], Yan-Hua Xiong [a], Yu-Qing Zhao [a], Zongpeng Xiu [a], Hui-Min Ren [a], Kai Zhang [a], Shun Duan [a,**], Ying Chen [b,***], Fu-Jian Xu [a,*]

[a] State Key Laboratory of Chemical Resource Engineering, Key Lab of Biomedical Materials of Natural Macromolecules (Beijing University of Chemical Technology), Ministry of Education, Beijing Laboratory of Biomedical Materials, Beijing Advanced Innovation Center for Soft Matter Science and Engineering, Beijing University of Chemical Technology, Beijing, 100029, China

[b] Department of Orthopaedic Surgery, China-Japan Friendship Hospital, Beijing, 100029, China

ARTICLE INFO

Keywords:
Antibacterial
Open fracture
Infection-responsive
Coating
Orthopedic medical device

ABSTRACT

The infections in open fracture induce high morbidity worldwide. Thus, developing efficient anti-infective orthopedic devices is of great significance. In this work, we designed a kind of infection-responsive long-term antibacterial bone plates. Through a facile and flexible volatilization method, a multi-aldehyde polysaccharide derivative, oxidized sodium alginate, was crosslinked with multi-amino compounds, gentamycin and gelatin, to fabricate a uniform coating on Ti bone plates via Schiff base reaction, which was followed by a secondary crosslinking process by glutaraldehyde. The double-crosslinked coating was stable under normal condition, and could responsively release gentamycin by the triggering of the acidic microenvironment caused by bacterial metabolism, owning to the pH-responsiveness of imine structure. The thickness of the coating was ranging from 22.0 μm to 63.6 μm. The coated bone plates (Ti-GOGs) showed infection-triggered antibacterial properties (>99%) and high biocompatibility. After being soaked for five months, it still possessed efficient antibacterial ability, showing its sustainable antibacterial performance. The *in vivo* anti-infection ability was demonstrated by an animal model of infection after fracture fixation (IAFF). At the early stage of IAFF, Ti-GOGs could inhibit the bacterial infection (>99%). Subsequently, Ti-GOGs could promote recovery of fracture of IAFF. This work provides a convenient and universal strategy for fabrication of various antibacterial orthopedic devices, which is promising to prevent and treat IAFF.

1. Introduction

Infection after fracture fixation (IAFF) is one of the most challenging complications in trauma surgery, which often leads to delay healing, permanent loss of function, amputation, and even death [1,2]. The reasons for fracture are a skeletal disorder [3–5], trauma [6–8], stress fractures [9], body weight [10], etc. Especially, open fracture could be induced by major trauma, which needs bone plates for osteosynthesis treatment. In open fracture, wounds are contaminated by microbes up to 65%, because the fractured bone tissues are exposed to the environment. Thus, open fracture usually prolongs recovery time and hospital stay. For third-degree open fracture, the infection ratio after osteosynthesis is up to 30% [11]. Such infections are mainly caused by bacteria, such as *Staphylococcus aureus* (*S. aureus*) [12]. Besides, during the course of fixation surgery, the surfaces of implants are susceptible to bacterial contamination from both skin and mucous membrane [13]. However, the traditional bone plates are made from stainless steel, titanium alloys, cobalt-chromium alloys, NiTi shape-memory alloys, polymeric materials [14–20], etc., which lack of antibacterial efficiency [21,22]. Systemic or topical antibiotic prophylaxis is a standard clinical practice in orthopedic surgery to treat bone plate-induced infections [23–26]. However, these strategies still have shortcomings, including induction of toxicity and antimicrobial resistance [27–30]. Therefore, the modified bone plate surfaces with the properties of minimal bacterial colonization,

Peer review under responsibility of KeAi Communications Co., Ltd.
* Corresponding author.
** Corresponding author.
*** Corresponding author.
E-mail addresses: duanshun@mail.buct.edu.cn (S. Duan), chenying7877@163.com (Y. Chen), xufj@mail.buct.edu.cn (F.-J. Xu).

https://doi.org/10.1016/j.bioactmat.2023.01.002
Received 21 October 2022; Received in revised form 19 December 2022; Accepted 3 January 2023

high biocompatibility, and release enough drug to eliminate the drug-resistant bacteria are eagerly needed.

Antibacterial surface functionalization is a key point to solve the problem of IAFF, because bacteria would contact with the surface of implants firstly. Many efforts had been done to develop implants with antibacterial surfaces, such as antifouling [31–33], contact-killing [34–36], and antibiotic-releasing surfaces [37–40]. Nevertheless, such antibacterial surfaces had some disadvantages, including short lifetime, toxicity, poor biocompatibility, drug resistance, etc [41–44]. Accordingly, both have antibacterial activity and biocompatibility requires the coatings to be "smarter", or have the "self-adaptive ability" [45].

To solve these problems, "self-adaptive antibacterial" implants were developed in recent years, which realized long-term antibacterial property and had low risk to induce drug resistance. "Self-adaptive ability" means materials could respond to chemical or physical signals and make changes spontaneously, such as temperature [46], salt concentration [47], light [48], and pH value [49]. Among them, pH-responsive polymers have attracted much attention due to their applications *in vitro* and *in vivo* biomedical fields and the biological relevance of pH regulation in organisms. In our previous study, we had developed a self-adaptive antibacterial surface by surface-initiated atom transfer radical polymerization (SI-ATRP), which could be responsive to bacterial infection by pH-responsive Schiff base structure [50]. The bacterial metabolism could produce acidic micro-environment [51,52] that could regulate antibiotic release to achieve on-demand administration. However, the reaction process of SI-ATRP was still complicated, which limited its application on biomedical devices. Furthermore, many other methods for prepare pH-responsive coatings were developed in recent years, such as electrostatic self-assembly, covalent grafting and biomimetic deposition [53–55]. These methods still had some concerns when they were used on bone implants, including short lifetime, low stability, and potential toxicity. Therefore, we expect to construct a biocompatibility and long-term self-adaptive antibacterial coating by a facile method.

Compared with synthetic polymers, natural polymers, particularly polysaccharides and their derivatives, were widely used for fabricating antibacterial coatings due to their excellent biocompatibility and biodegradability [56]. For example, sodium alginate (SA) is one of the natural polysaccharides with good biocompatibility. Gelatin, another kind of natural polymer, has excellent biocompatibility, plasticity, cell affinity and good film-forming property, which is also beneficial to improve the performances of the antibacterial coatings. To facilely construct natural polymer-based coatings, volatilization method is a more versatile and convenient method than SI-ATRP. As a one-step method, it could be applied on various surfaces. Therefore, it is feasible to construct a self-adaptive antibacterial coating on the surfaces

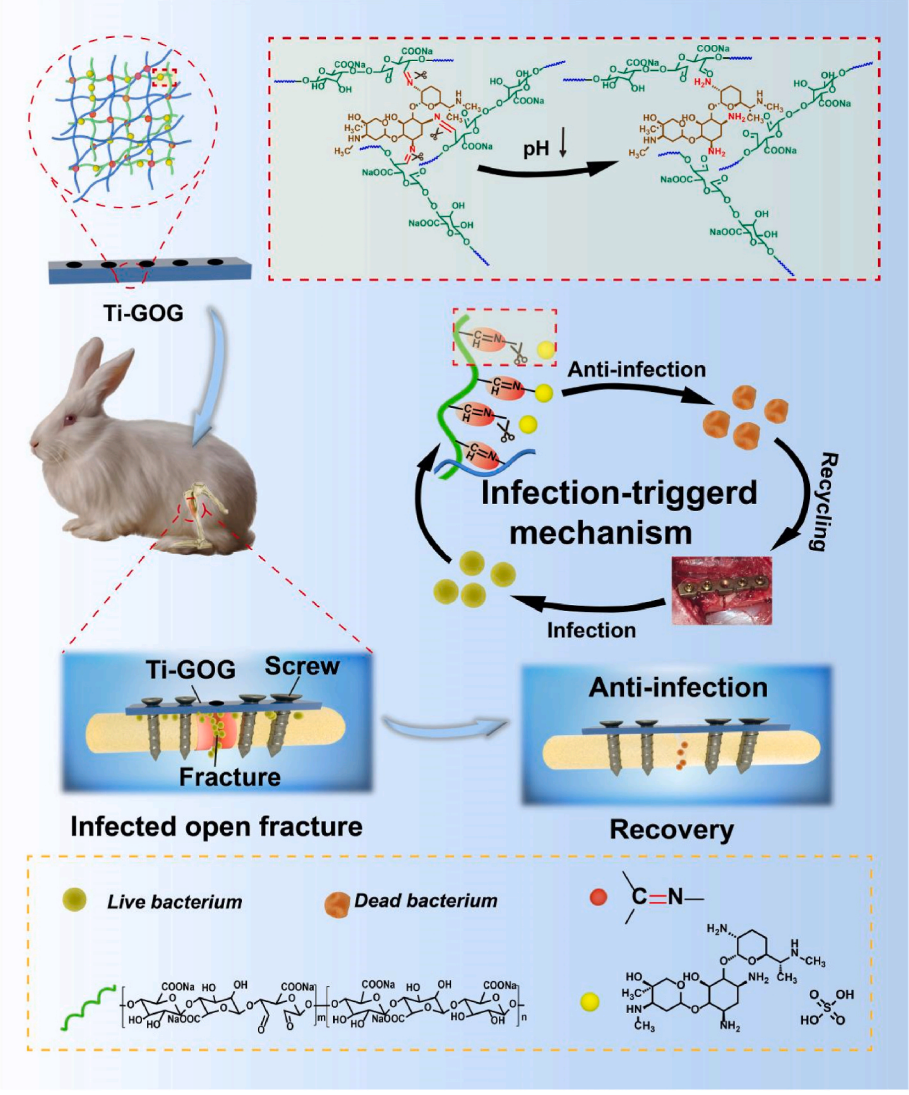

Scheme 1. Schematic illustration for the preparation and properties of Ti-GOG implant.

of the implants by this facile and universal method.

In this work, we developed a kind of antibacterial bone plate with the properties of minimize bacterial colonization, high biocompatibility, and infection-responsive antibiotic release (Scheme 1). Oxidized SA (OSA), which was prepared by SA and sodium periodate ($NaIO_4$) to introduce aldehyde groups, covalently loaded gentamycin sulfate (GS) by pH-responsive Schiff base structures. The bacterial metabolism could produce acidic micro-environment that could regulate antibiotic release to achieve on-demand administration. The implants were modified with the pre-coated solution which contained gelatin, OSA and GS by facile volatilization method. The coating on the modified bone plates (Ti-GOGs) was cross-linked by glutaraldehyde (GA) to further improve the long-term stability. The highly stable, self-adaptive antibacterial properties were investigated by *in vitro* antibacterial experiments and drug loading and release analysis. The *in vivo* anti-infection performances were evaluated by an infected open fracture model. The present work provided a facile, universal strategy for the clinical treatment of IAFF, which could be applied to various types of implants with various shapes.

2. Results and discussion

2.1. Physical and chemical properties of coating-functionalized Ti bone plates (Ti-GOGs)

Ti samples were washed with NaOH at 60 °C, and washed alternately with ethanol and deionized water for three times. Polydopamine (PDA)-modified Ti samples (Ti-PDA) were prepared by self-polymerization of dopamine (DA) on the Ti surface. OSA with oxidation degrees of 15%, 50% and 70% were prepared by SA and $NaIO_4$, named as OSA1, OSA2 and OSA3, respectively (Fig. S1, Supporting Information). Due to the high steric hindrance of sodium alginate, 70% is the maximum degree of oxidation. The pre-coated solution was prepared with gelatin, GS and OSA. Ti-PDA was soaked into the pre-coated solution, and then dried slowly at 40 °C to form coating-functionalized bone plates (Ti-GOG1, Ti-GOG2, or Ti-GOG3). At last, the samples were soaked into 2.5% glutaraldehyde solution in phosphate buffer saline (PBS) to crosslink the coating, and washed with ethanol and deionized water for three times (Scheme 1).

The synthesis process of the samples (Fig. S2a, Supporting Information) was confirmed by scanning electron microscopy (SEM), X-ray photoelectron spectroscopy (XPS), atomic force microscope (AFM), and

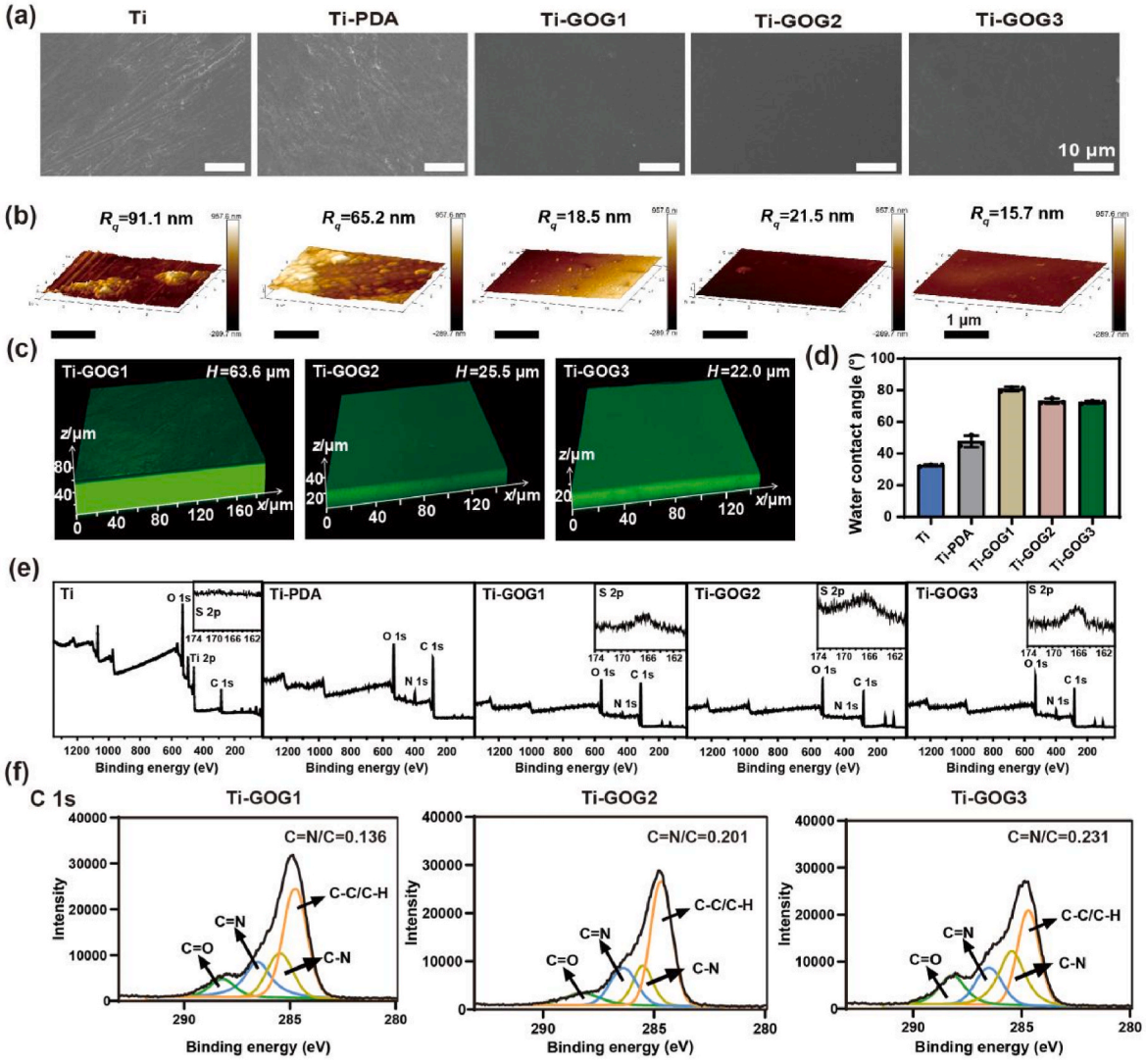

Fig. 1. Physical and chemical properties of coating-functionalized Ti bone plates. a) SEM images and b) AFM images of Ti, Ti-PDA, Ti-GOG1, Ti-GOG2, and Ti-GOG3 surfaces; c) representative CLSM 3D-scanning images of Ti-GOG1, Ti-GOG2, and Ti-GOG3; d) water contact angles and e) XPS wide-scan spectra of Ti, Ti-PDA, Ti-GOG1, Ti-GOG2, and Ti-GOG3, S 2p core-level spectra of Ti, Ti-GOG1, Ti-GOG2, and Ti-GOG3; f) C 1s core-level spectra of Ti-GOG1, Ti-GOG2, and Ti-GOG3.

the confocal laser scanning microscope (CLSM). The surface morphologies of the pristine Ti and modified Ti were observed by SEM and AFM. After modification of dopamine, the color of the Ti changed into deep brown. A visible polymer layer could be seen on the surface of Ti-GOGs (Fig. S2b, Supporting Information). As shown in Fig. 1a, the coatings were flat and dense. After surface functionalization, the morphologies of functionalized samples were changed from rough to smooth, which was further verified by AFM. The AFM images showed the surface roughness of modified samples decreased (R_q = 65.2 nm, 18.5 nm, 21.5 nm and 15.7 nm of Ti-PDA, Ti-GOG1, Ti-GOG2 and Ti-GOG3, respectively, *vs* 91.1 nm of Ti, Fig. 1b). The surface of pristine Ti was rough after pretreated. After modification, the coating covered the rough surface of pristine Ti and reduced the roughness. Because the coatings were formed via Schiff base reaction, many C═N bonds existed in the molecular structure of the Ti-GOG coatings. The *n*-π^* transitions of C═N bonds in the Schiff base could produce the auto-fluorescent property [57,58]. Thus, the thicknesses of the Ti-GOG samples were measured by a visualized method with CLSM. The thickness of the coatings on Ti-GOG1, Ti-GOG2 and Ti-GOG3 were 63.6 μm, 25.5 μm and 22.0 μm, respectively (Fig. 1c). The results of SEM, AFM and CLSM also showed the good uniformity of Ti-GOGs. With the increasing oxidation degrees of OSA, the thickness of coatings decreased, which was due to the increased degree of crosslinking. The obvious changes of water contact angles also proved the successful formation of coating (Fig. 1d). To evaluate the GA further increased the degree of crosslinking, the Ti-GOG3 was selected as a representative sample to observe. Attenuated total refraction Fourier transform infrared (ATR-FTIR) spectroscopy was displayed in Fig. S3 before (Ti-GOG3/GA-) and after (Ti-GOG3/GA+) the introduction of GA. The absorption at typical amino I (green frame) in the Ti-GOG3/GA+ was obviously stronger than that of Ti-GOG3/GA-, which indicating the increased degree of crosslinking was owning to the increased C═N structure.

The surface chemical compositions of Ti-GOGs were analyzed by XPS (Fig. 1e). After modification with PDA, the signal of Ti was decreased significantly. The intensity of C 1s and N 1s signal increased obviously. The decrease of the N 1s and the disappearance of the Ti 2p could be observed after the surface modification of the coating, indicating that the surface coating was successfully modified. After coating formation, a new characteristic peak appeared at the binding energy of 166 eV (S 2p), which was attributed to sulfur element of GS. Also, the C 1s signals at the binding energy of 286 eV of Ti-GOG1, Ti-GOG2 and Ti-GOG3 were attributed to the C═N bond in the Schiff base structure, proving the successful modification of GS (Fig. 1f). Because gelatin is a large molecule, the reaction rate between GS and OSA is higher than that of gelatin. These results demonstrated the coatings have been successfully crosslinked, and GS was loaded by Schiff base reaction.

2.2. In vitro biological performances

By controlling the degrees of oxidation, a series of Ti-GOG samples with different amounts of GS were prepared. The GS-loading dosages in the coatings were calculated by the *o*-phthalaldehyde method. The GS-loading dosages of Ti-GOG1, Ti-GOG2, Ti-GOG3 with the area of 0.8 cm^2 were 0.64, 1.25 and 1.57 mg cm^{-2} (Fig. 2a). The amounts of loaded GS increased with the increasing oxidation degrees of OSA. The higher degree of oxidation possessed richer active sites, which could react with and load more GS to achieve sustainable antibacterial response.

The bacteria-responsive antibacterial coating could achieve antibacterial ability on demand and reduce the possibility to induce drug resistance. Bacterial metabolism can produce a weakly acidic microenvironment, which has a pH value of 5.0–6.5 [59–61]. Such micro-environment could lead to the breakage of Schiff base bonds and release GS to kill bacteria responsively, which present a self-adaptive antibacterial behavior. In order to prove the self-adaptive release of GS from Ti-GOGs, Ti-GOG3 was selected as a representative sample to study the release behavior of GS under neutral and weakly acidic conditions. The pH value of 5 was selected to simulate the microenvironment of severe infection. The samples were soaked into PBS (pH = 7.4) and acetic acid-sodium acetate buffer solution (HAc-NaAc, pH = 5.0). At the preset time points, the extracts were taken for GS concentration measurement. The results showed that the GS was gradually released from Ti-GOG3 under the weakly acidic condition, while the

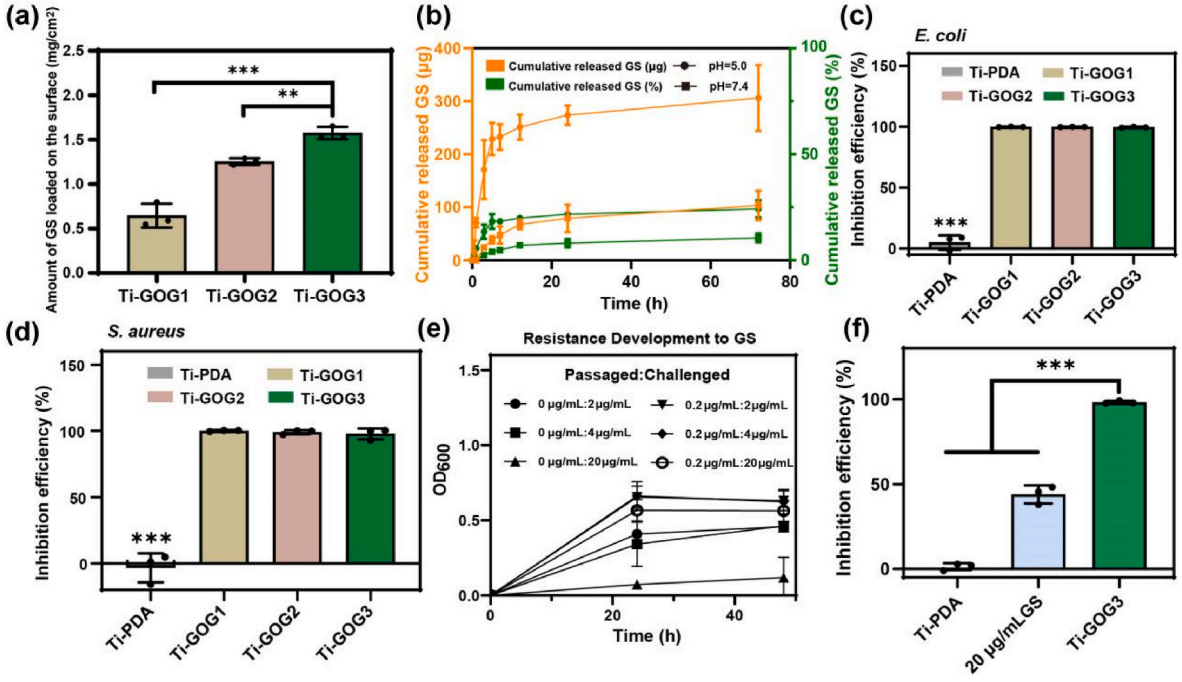

Fig. 2. Self-adaptive antibacterial analysis. a) The GS loading dosages in Ti-GOG1, Ti-GOG2 and Ti-GOG3; b) cumulative masses and ratios of released GS from Ti-GOG3 under pH = 5.0 and 7.4 (orange color: cumulative released mass; green color: cumulative released ratio; round icons: pH = 5.0; square icons: pH = 7.4); antibacterial efficiencies of Ti-PDA, Ti-GOG1, Ti-GOG2 and Ti-GOG3 against c) *E. coli* and d) *S. aureus*; e) drug resistance development of *S. aureus* by successive passage in low concentration of GS; f) the inhibition efficiency of Ti-PDA, 20 μg mL^{-1} of GS and Ti-GOG3 against induced drug-resistant *S. aureus*.

accumulative release amount in neutral condition was 66.13% lower than that in weak acid at 72 h. After 72 h, there was about 75.79% of GS still remained under acidic condition (Fig. 2b). The imine bond is a dynamic construction, when it reaches a dynamic equilibrium in acidic condition, it is no longer released [62]. In this situation, the GS will release in the stimulation of a new acidic environment, which indicating sustainability in long-term antibacterial activity. Under neutral condition, the rate of GS release was slower than that of acidic condition. GS remained 89.44% after 72 h of soaking in PBS, because the chemical stability of Schiff base structure prolonged the lifetime of the antibacterial coating. In the antibacterial assay, all the Ti-GOG samples showed high antibacterial efficiencies (over 99%) against *E. coli* (Fig. 2c) and *S. aureus* (Fig. 2d). The above results proved that the Ti-GOG3 had self-adaptive GS release profile, which could be utilized for antibacterial therapy.

Antibiotic resistance is one of the major challenges facing modern medicine worldwide [63]. Drug resistance might be induced by existence of low-dose antibiotics for long time [64]. To evaluate the antibacterial property of Ti-GOGs against induced drug-resistant bacteria, Ti-GOG3 was selected as a representative sample. *S. aureus* was successively cultured for 19 days under a GS concentration of 0.2 μg mL^{-1}. This concentration was much lower than the minimal inhibitory concentration (MIC) of GS, which could simulate the problem of inducing drug resistance of antibiotic treatment [64]. Then, bacteria were cultured under the concentration of 4 μg mL^{-1} (MIC concentration, Fig. S4, Supporting Information), 2 μg mL^{-1} and 20 μg mL^{-1} (the dose of 10 × and 100 × passage concentration) for 48 h (Fig. 2e). No antibacterial effect was observed even at the 100 × dose, indicating that low-dose GS could induce bacterial drug resistance in a long period. In order to prove the antibacterial effect of the Ti-GOGs on the drug-resistant bacteria, the Ti-GOG3 was co-cultured with the resistant bacteria (Fig. 2f). The results showed that even if the bacteria produced drug resistance, the Ti-GOG3 (1.23 mg) still had excellent antibacterial efficiency compared with GS (20 μg mL^{-1}, 100 × passage concentration). It is because that the resistant bacteria could still produce a weakly acidic micro-environment, which led to the breakage of C═N bonds and released enough GS until complete elimination of the drug-resistant bacteria.

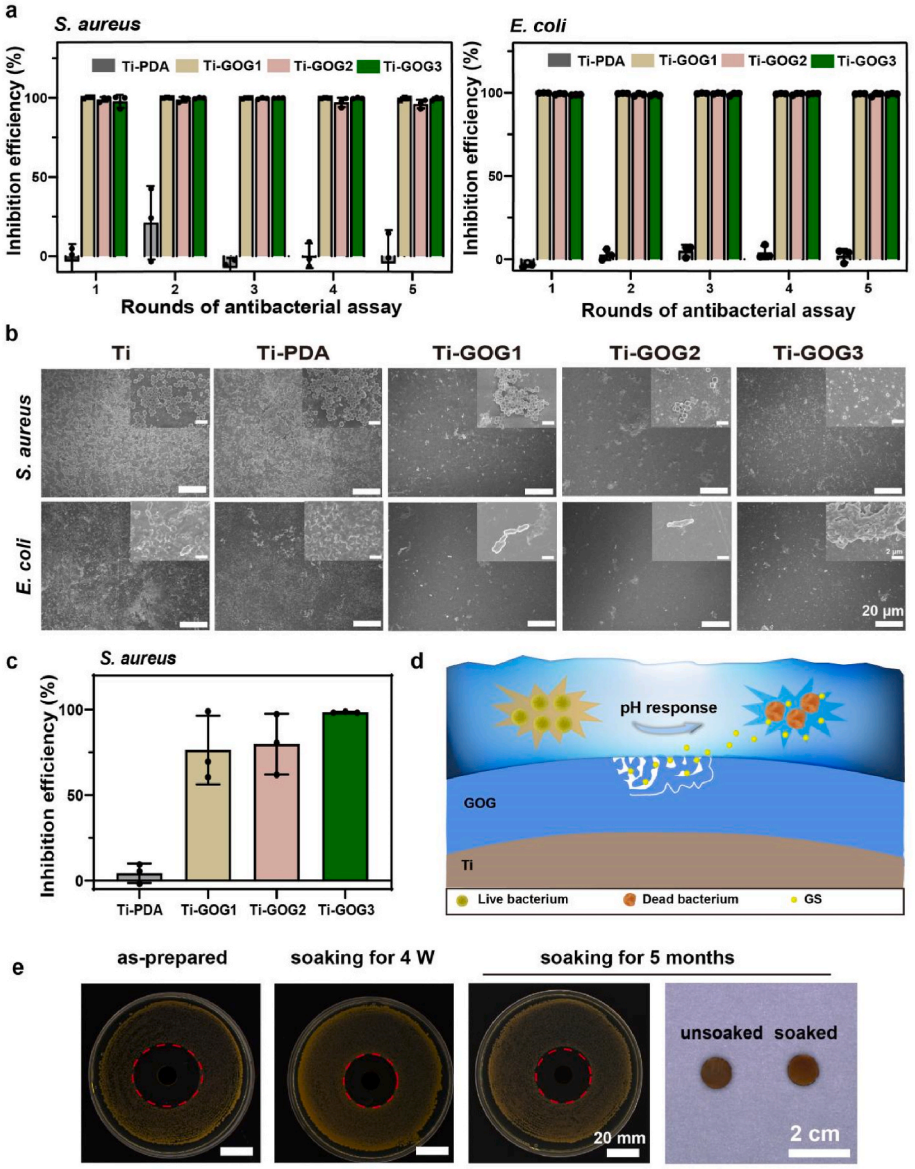

Fig. 3. Antibacterial analysis. a) Cycling antibacterial assay against *S. aureus* and *E. coli* in liquid culture media; b) SEM images of sample surfaces after cycling antibacterial assay; c) antibacterial assay against high density of *S. aureus*; d) schematic illustration for the antibacterial activity of Ti-GOGs; e) inhibition zones against *S. aureus* of as-prepared and soaked Ti-GOG3 samples soaked in PBS for 4 W and 5 months.

In order to confirm the mechanism of self-adaptive antibacterial behavior, Ti-GOG3 was reacted with excessive amount of sodium cyanoborohydride ($NaBH_3CN$) as a control group (denoted as Ti-GOG3-R) in which the C═N bonds between GS and OHA were reduced into chemically stable C–N bonds. The C–N bonds could not be broken by acidic environment in Ti-GOG3-R and GS could not release from the coating under acidic environment. Therefore, Ti-GOG3-R showed no antibacterial ability (Fig. S5, Supporting Information). This result proved that the antibacterial ability was caused by the release of GS due to the acid-triggered breakage of C═N bonds from Schiff base reaction.

In the clinical practice of orthopedics, the morbidity of delayed and recurrent infections is high. Therefore, the antibacterial orthopedic implants should have long lifetime, which is beneficial for long-term anti-infection application. In order to verify the long-term antibacterial properties of Ti-GOGs, Gram-positive bacteria (*S. aureus*) and Gram-negative bacteria (*E. coli*) were used to evaluate the cycling antibacterial properties. The cycling antibacterial tests were carried out for five times to determine the long-term antibacterial properties (Fig. 3a). The results showed that Ti-GOG1, Ti-GOG2 and Ti-GOG3 had constant antibacterial ability for five times, indicating that Ti-GOGs could resist recurrent infection. By measuring the GS loading dosages, the samples in all the groups were loaded with high amounts of GS. Therefore, all the samples showed good antibacterial performances against the bacteria with low density. And the self-adaptive antibacterial coating could achieve antibacterial ability on demand and avoid the explosive release of GS, which prolonged the lifetime of Ti-GOGs. Furthermore, the adhesion of debris of bacteria could contaminate the surface on bone plate, which is harmful to the biological performances. Thus, the sample surfaces after cycling antibacterial tests were observed by SEM (Fig. 3b). A large number of bacteria adhered on the surface of pristine Ti and Ti-PDA. However, the surfaces of Ti-GOGs could effectively reduce the adhesion of bacteria, showing antifouling property. On the surface of Ti-GOG3, only bacterial debris were observed, indicating its high bactericidal efficiency. Fig. 3b showed the morphology of adhered bacteria in the Ti-GOG1, Ti-GOG2 and Ti-GOG3 groups showed deformed and shrunken, which indicated the bacteria have been inactivated, which is consistent with the results of antibacterial ratio (Fig. 3a). To evaluate the response to implant-associated severe infection, the density of *S. aureus* was increased to 10^7 CFU/mL (Fig. 3c). Under this high bacterial density, Ti-GOG3 still had excellent antibacterial efficiency, which was better than those of Ti-GOG1 and Ti-GOG2. The Ti-GOG3 loaded the largest amount of GS, because the highest degree of oxidation possessed abundant reactive sites, which possessed the highest antibacterial activity. Therefore, Ti-GOG3 was capable to fight with severe infections.

Fig. 3d illustrated the mechanism of the antibacterial properties of the Ti-GOG coatings. To fight with delayed infection, the bone plates should have stable antibacterial potential after a long-term therapeutic process. Due to the good antibacterial ability against severe infection, Ti-GOG3 was selected as a representative sample to test the long-term antibacterial ability after soaking in PBS for four weeks and five months, respectively (Fig. 3e). After being soaked for a long time, Ti-GOG3 maintained the pristine morphology. Moreover, the soaked samples still showed high antibacterial efficiency, owning to the stability of covalent linkage between GS and OSA. This result indicated that Ti-GOG3 could have long-term antibacterial ability during the long serving period of bone plates. The antibacterial results suggested that Ti-GOG3 had the best *in vitro* antibacterial performances, which could be used to inhibit recurrent and delayed infections.

Orthopedic implants should have good biocompatibility. To evaluate the biocompatibility of the Ti-GOG samples, hemolysis and cell toxicity assays were performed. The results showed that the hemolysis ratios of all samples were less than 5%, indicating that the samples had good blood compatibility (Fig. 4a). To evaluate the blood adhesion on the surfaces, the samples were immersed into the fresh whole blood or platelet-rich plasma (PRP), and the adhered blood cells were observed by SEM (Fig. S6, Supporting Information). The amount of adhered blood cells on the Ti-GOG3 surface was lower than those of Ti, Ti-PDA, Ti-GOG1, and Ti-GOG2. The same tendency between Ti-GOGs was observed in the protein adhesion test (Fig. S7, Supporting Information). Above-mentioned results showed that Ti-GOG3 could effectively reduce adhesion of blood cells and bovine albumin (BSA), which was consistent with the results of antifouling test against bacteria (Fig. 3b). As a temporary implant, the *in vitro* biocompatibility of Ti-GOGs was tested by cell biocompatibility in 24 h according to ISO10993. To evaluate the biocompatibility, an osteoblast cell line, MC3T3-E1, was selected to determine the cytotoxicity (Fig. 4b). The relative cell viability of each group was higher than 70%, which demonstrated that all samples had good cell viabilities. Because polysaccharides and gelatin have good cell affinity, the relative cell viabilities of Ti-GOG1, Ti-GOG2 and Ti-GOG3 were higher than those of pristine Ti. The above results showed that the Ti-GOG3 had good biocompatibility and optimized antibacterial properties, which could be used for further *in vivo* anti-infection study.

2.3. *In vivo* anti-infection performances

To construct the animal model, the Japanese rabbits were used to make an open fracture at the tibial midshaft (Fig. S8, Supporting Information). Animal studies were approved by the Ethical Committee of China-Japan Friendship Hospital and conducted according to legal agreement. Moreover, *S. aureus*, the most common pathogen causing implant-associated infections, was inoculate to the bone plate to simulate IAFF. Ti-GOG3 was implanted to fix the open fracture with screws. In order to be close to the clinic practice, Ti bone plants were used in the control group of animal experiments, because Ti bone plants were widely used in the clinical treatment of bone fracture. After operation, the recovery of wounds was observed. Ti group showed significant

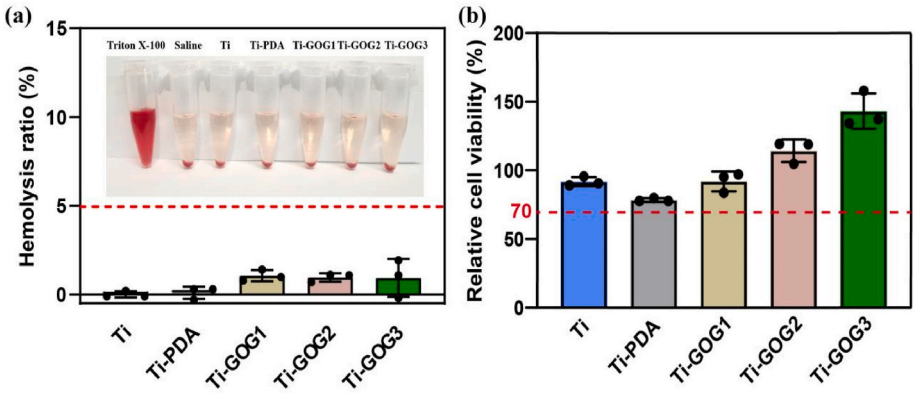

Fig. 4. Biocompatibility analysis. a) Hemolysis ratios and b) cytotoxicity of Ti, Ti-PDA, Ti-GOG1, Ti-GOG2 and Ti-GOG3.

swelling from 1 to 4 d (marked by red circles). At 7 d, heavy pyogenic fluids (marked by red circles) were observed in the Ti group, indicating a severe infection at the sites of open fracture. At 14 d, the infection persisted and the wound exposed, which could further exacerbate infection and delay the recovery of the fracture. On the contrary, the rabbits in Ti-GOG3 group were normal from 1 d to 14 d, indicating that the wound recovered well and no obvious infection occurred (Fig. 5a).

For further evaluation of the infection, whole blood was collected from the ear-vein of rabbits at specific time point, and blood routine examination was performed. The amounts of neutrophils (NEUT) and white blood cells (WBC) and the concentrations of C-reactive protein (CRP) were tested to determine the levels of inflammatory response. The CRP and WBC could assess the strength of the immune response, and NEUT which had certain specificity to bacteria could reflect the situation of infection. A stress response to postoperative tissue damage could lead to a surge in WBC, CRP and NEUT values. However, the stress response could decrease rapidly after operation. However, the stress response could decrease rapidly after operation. At 1 d, the CRP values of Ti-GOG3 and Ti increased significantly (Fig. 5b). But after 4 d, the CRP values of the Ti-GOG3 group were significantly lower than those of the Ti group, and backed to normal, indicating that the infection was inhibited in Ti-GOG3 group. The WBC (Fig. 5c) and NEUT (Fig. 5d) values of Ti group were significantly higher than those of Ti-GOG3 group, which still staying at a high level at 7 d. The indexes of the Ti group were significantly higher than those of the Ti-GOG3 group, demonstrating that the presence of stress response might be caused by bacteria infection at the same time. Therefore, these results indicated that the inflammatory responses in Ti-GOG3 group were lower than those in Ti groups.

In order to verify the presence of bacterial infection, the whole blood was centrifuged to detect the interleukin 6 (IL-6, Fig. 5e) and tumor necrosis factor α (TNF-α). IL-6 can directly reflect the intensity of infection, and TNF-α is proinflammatory cytokines in the early stages of infection, which shows high sensitivity to bacteria. The levels of TNF-α in Ti group increased significantly after operation and still maintained at a high level at 14 d, indicating severe infection occurred in Ti group. The TNF-α values of Ti-GOG3 had been maintained at a lower level (Fig. 5f). These results meant that Ti-GOG3 had excellent anti-infection property, which was attribute to the self-adaptively released GS. In order to verify that the release of antibiotics was limited at the local infected sites and had no systematic side effect, blood concentrations of GS were detected at the present time points (Fig. 5g). The results showed that blood concentrations of GS did not increase at all time points, which could effectively avoid the toxicity caused by the large amount of GS. As mentioned above, the Ti-GOG3 group had excellent anti-infection performance and biosafety, and could be effectively used in orthopedic implant materials.

To further evaluate the anti-infection properties of Ti-GOG3,

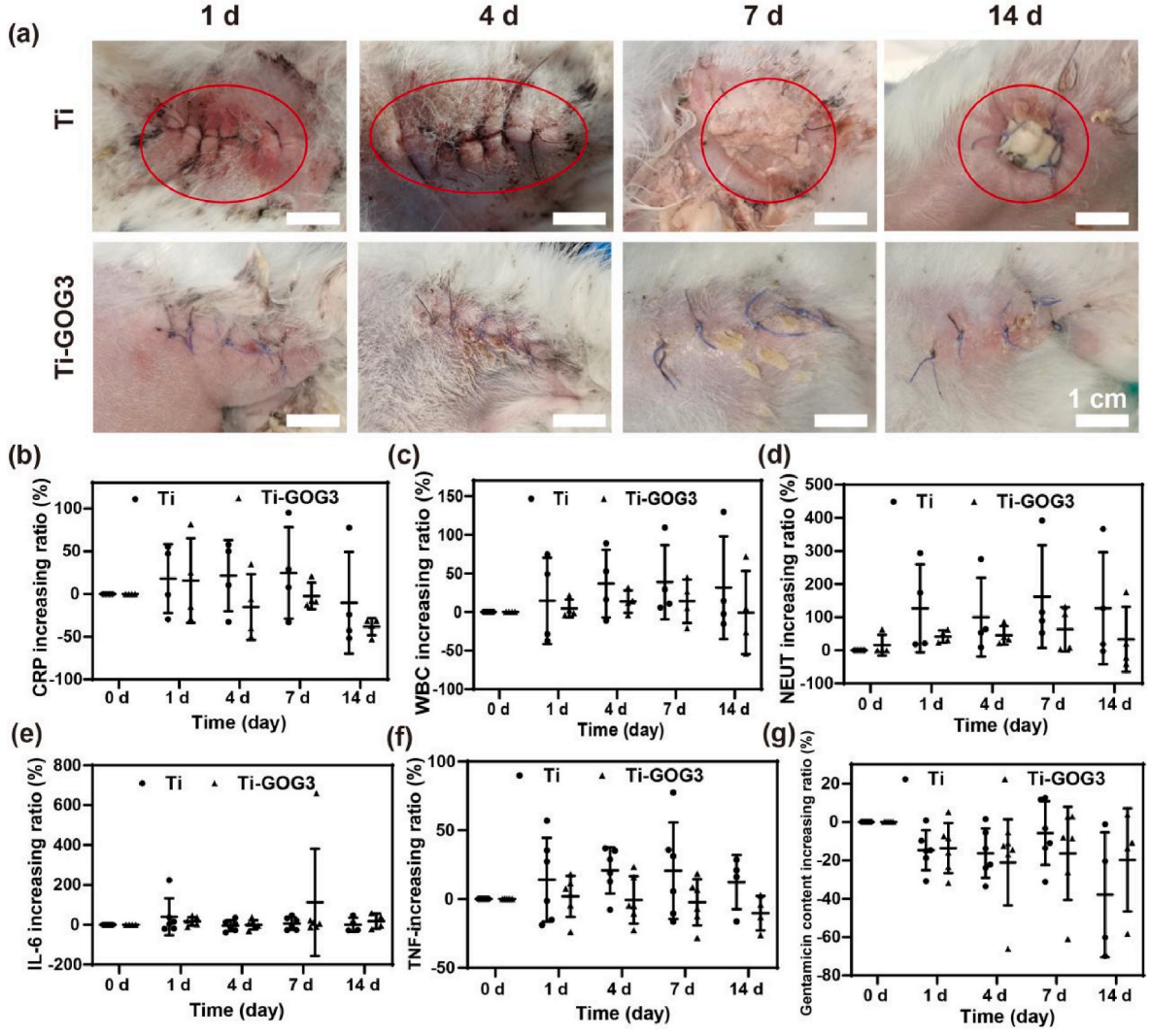

Fig. 5. General superficial views and blood routine examination. a) General superficial views of the bone fracture areas of rabbit models; the increasing ratios of b) CRP, c) WBC, and d) NEUT from 0 to 14 d; the increasing ratios of e) IL-6, f) TNF-α and g) blood concentration from 0 to 14 d.

bacterial culture was performed. The tissues around the bone plate were collected and homogenized at 1 and 4 W after operation. The homogenates were spread on standard ager plates and incubate at 37 °C for 24 h (Fig. 6a). The numbers of bacteria colonies on the surface of the Ti-GOG3 group were significantly lower than those of the Ti group, which could effectively kill 99.9% of the bacteria (Fig. 6b). The Ti group still had a large number of bacteria in the tissues at 4 W, indicating that the Ti group had a chronic infection, which might delay fracture healing. These results demonstrated that the Ti-GOG3 group could effectively kill bacteria in the early stage of infection.

There were heavy pyogenic fluids in the muscle tissue in Ti group for the severe bacterial infections, while no inflammation was observed in Ti-GOG3 group (Fig. S9, Supporting Information). Furthermore, the inflammatory response of the tissue was assessed by histological analysis. The tissues around the plates were observed by hematoxylin-eosin (H&E) staining at 1 and 4 W after operation (Fig. 6c). At 1 W, the Ti group could observe obviously inflammatory cells (neutrophils, lymphocytes, etc.), which proved that acute inflammatory reaction and strong immune response occurred. At 1 and 4 W, most of the cells of the Ti-GOG3 group were normal and did not occur inflammatory reaction. The numbers of inflammatory cells in Ti group are significantly higher than that of Ti-GOG3 group at 4 W (Fig. 6d), indicating that the inflammatory reaction and immune response still exist, and the infection period and fracture healing process were prolonged. The histological results further proved that the Ti-GOG3 group had excellent *in vivo* antibacterial properties and could effectively deal with implant-related infections.

2.4. Recovery of infected open tibial fracture in animal models

To verify the effects of anti-infection properties on fracture recovery, experimental animals in each group were sacrificed at 4 and 8 W after operation to observe the fracture sites (Fig. 7a). For the Ti group, the cortical locking screws appeared loosen and moved at 4 W (Fig. 7b). The loose of the cortical locking screws caused rejection reaction and formed cysts (Fig. S10, Supporting Information). The moved screw with sharp edges rubbed tissue caused tissue damage, which triggered a more intense inflammatory response. The mild pyogenic fluids were still observed at 8 W, indicating that the Ti group might appear chronic infection (Fig. S9, Supporting Information). When the bone plates were removed at 8 W, the coatings still firmly combined with the bone plate, which were transformed from a light brown to bright yellow over time (marked by red arrows in Fig. S11a, Supporting Information). This result indicated that the biodegradation time of the coatings was longer than 8 W, which ensure they had long service time. Then, the binding force between the coating and the substrate was measured by the scratch testing, which was determined as 9.96 N (Fig. S11b, Supporting Information). These results along with the *in vitro* stability test (Fig. 3e) verified that the Ti-GOG3 had "long-term" stability, which ensured that Ti-GOG3 could keep the anti-infection property during the service time of bone plate. The above results showed that the Ti-GOG3 group had long lifetime to inhibit infection and avoided the cortical locking screws appearing loosen and moved phenomenon.

The fracture line healing was observed by X-ray photograph. In Ti group, enlarged fracture wounds (marked by red dotted frame, Fig. 7c), multiple fractures, dislocated fractures and bone marrow cavities at both

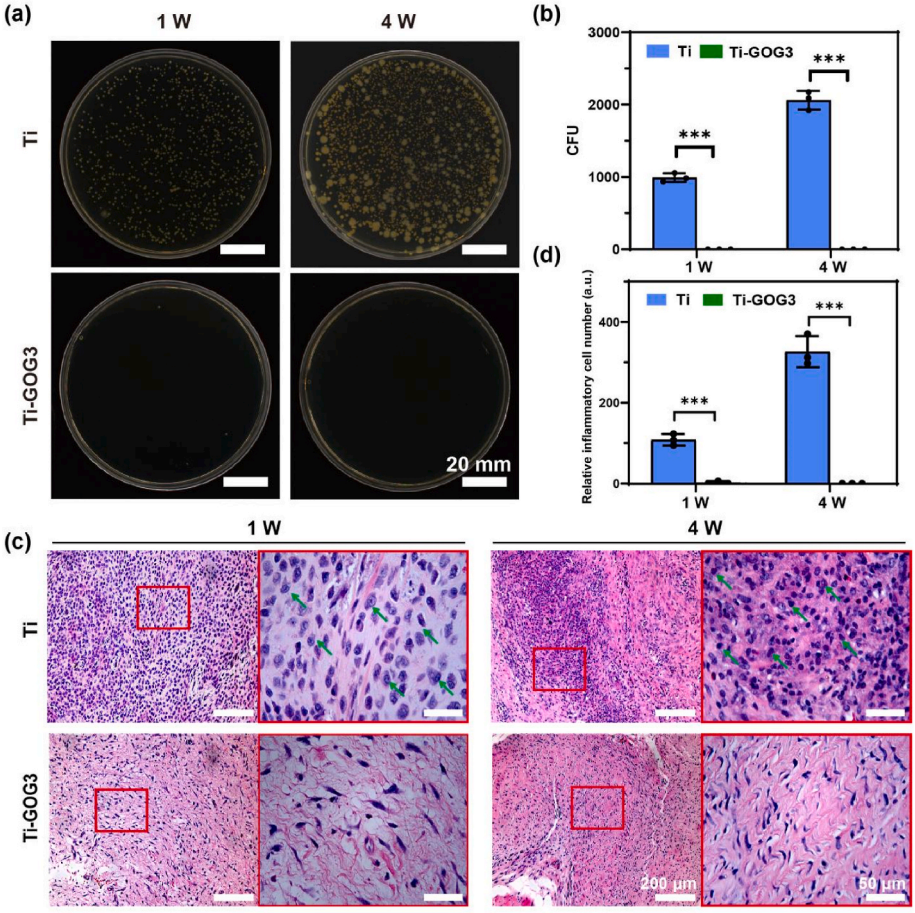

Fig. 6. ***In vivo*** **tissue inflammatory reaction was evaluated by histological analysis.** a) Representative images and b) counting of *S. aureus* colonies in the Ti and Ti-GOG3 groups at 1, and 4 W after operation; c) Histological examination by hematoxylin-eosin (H&E) staining of the tissues around the implants of Ti and Ti-GOG3; d) relative inflammatory cell number at 1 and 4 W after operation (green arrows indicating inflammatory cells). Data are presented as means ± SD (***P < 0.001).

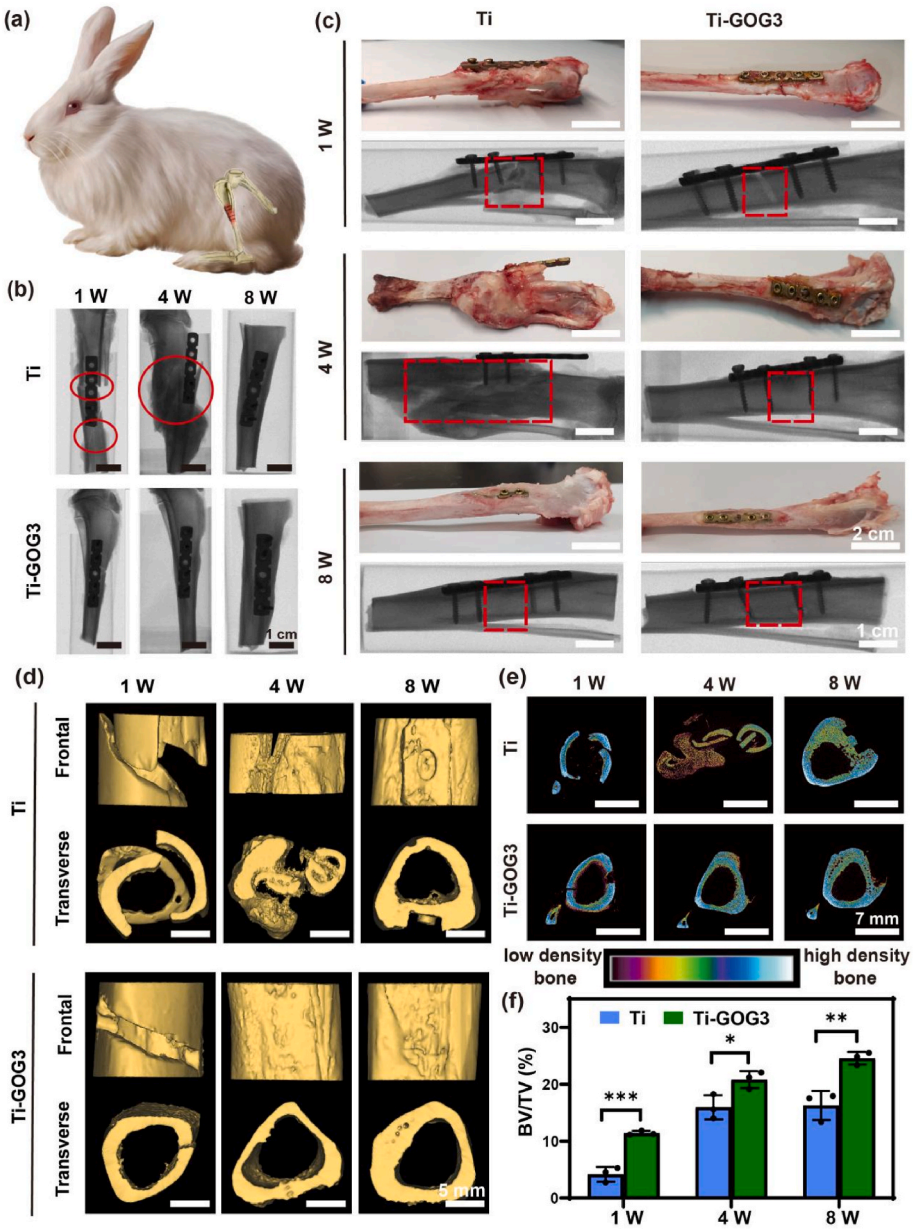

Fig. 7. Recovery of infected open tibial fracture. a) Illustration of IAFF animal modal; b) and c) X-ray images of the fractured bone of Ti and Ti-GOG3 after 1, 4 and 8 W of implantation (the fracture lines are highlighted by red dotted frame); d) frontal and transverse views of the 3D-reconstructed images; e) representative CT images and density mappings of the section which closest to the fracture line; f) quantitative analysis of BV/TV. Data are presented as means ± SD (*P < 0.01, **P < 0.05, ***P < 0.001).

ends of fracture line (marked by red circle, Fig. 7b) were found. The fracture line healed at 8 W, but the tibia was deformed compared with the Ti-GOG3 group (Fig. S12, Supporting Information). The severe infection in Ti group caused screws loosening, and even shedding at 1 and 4 W. Because the complement was activated by severe infection, inflammatory cells were recruited. Meanwhile, complement activation would have an impact on local inflammation by attracting phagocytes [65–68]. Thus, the stability of bone plate fixation was not maintained. The bone on both sides of the fracture line was misaligned and a large number of calluses were formed, which resulted in the thickening of cortical bone and the formation of deformed bone. Therefore, severe infection delayed fracture healing. In the Ti-GOG3 group, the fracture line was apparent at 1 W, the individual healed completely at 4 W, and completely healed at 8 W. The fracture recovered well. There was no phenomenon of screws migration, fracture wounds enlargement, chronic infection and tibia deformation in Ti-GOG3 group. These results indicated that Ti-GOG3 could eliminate infections at early stage of infected open fracture, which was beneficial for recovery of bone fracture at late stage. The high GS loaded and double cross-linking system prolonged the lifetime and stable antibacterial properties of the coating caused these results.

For the further evaluation of fracture healing quality, micro-CT analysis was performed (Fig. 7d and e). The sections closest to the fracture line were selected and processed into pseudocolor images to identify the differences in density. Native bone and new-formed bone were represented in blue/white and red/purple. In the Ti group, no new-formed bone was observed around the fracture line at 1 W (Fig. 7e). A large number of low-density bones were observed between fracture spaces at 4 W, indicating more new bones formed. More bones that represented in yellow/green were observed at 8 W, suggesting the process of transition from new-formed bone to native bone. In comparison with the Ti group, the density mappings showed that less bones with low density were observed around the fracture line at 1 W, indicating that bacterial infection could hinder the formation of new bone tissues. More bone tissues with high density were observed at 4 and 8 W, suggesting that the Ti-GOG3 group formed more new bones as well as better bone integration. Therefore, compared to Ti, the Ti-GOG3 group could inhibit bacterial infection by self-adaptively released GS to

promote the formation of new bone.

To visualize bone regeneration, the fracture sites were three-dimensionally (3D) reconstructed (Fig. 7d). Multiple fractures of the fracture line in the Ti group increased the fracture areas and a slight misalignment of both sides of the fracture line was observed form the transverse view at 1 W. After 4 W of surgery, the cross section of the tibia increased significantly. From the transverse view, the two sides of the bone were completely misplaced, and a large number of new bones were formed between the native bones. The native bone was squeezed and distorted, the section of the native bone was significantly reduced and the deformed bone formed. It suggested that severe infection caused screws shedding and bone plate losing fixation, and seriously affected the quality of fracture healing. The fracture line was apparent at 1 W in the Ti-GOG3 group. But there was no fracture line enlargement and dislocation growth. The fracture line healed in the Ti-GOG3 group at 4 and 8 W, and in the Ti group at 8 W. These results showed that mild infection would delay the healing of the fracture line, but severe infection and infection-associated inflammation would seriously affect the quality of fracture healing. The bone volume/total volume (BV/TV) was the index of osteogenic capacity. The new bone formation was evaluated in the volume of interest (VOI), which was around the fracture line into the cubes of 1 mm × 1 mm × 1 mm. The values of the BV/TV for the Ti-GOG3 group were higher than those for the Ti group at each time point (Fig. 7f), indicating that the osteogenic ability of Ti-GOG3 group was better. Ti-GOG3 could promote the fracture recovery in the case of infection by inhibiting inflammation and preventing bone resorption through antibacterial treatment. In addition, Ti-GOG3 could be used immediately after open fracture because of its high anti-infection property, which also could improve the recovery of open fracture. The above results showed that Ti-GOG3 group with high GS loaded could significantly inhibit mild or severe infection by self-adaptive release, and further to be beneficial for fracture healing.

After operation, in order to analyze the detailed histological results, the bone tissues at the fracture site were observed by hematoxylin and eosin (H&E) staining (Fig. 8a), toluidine blue (Fig. S13, Supporting Information), and Masson's trichrome staining, respectively (Fig. 8b). At 1 W, a large number of new bones formation were observed at the fracture line of the Ti-GOG3 group. The fracture line was filled with chondrocytes and osteoblasts (marked by red and yellow arrows), forming cartilage hyperplasia area at 4 W. Both sides of the bone were connected, and no broken fracture line was observed. The fracture line completely healed at 8 W. And the cortical bone mineral density was high (marked by purple arrows), which demonstrating that the fracture recovered well. No inflammation-associated cells were observed in the Ti-GOG3 group. However, obvious bone nonunion phenomenon and inflammation-associated cells (highlighted by orange frame) could be observed in the Ti group at 1 W, suggesting that occurred bacterial infection. There was no osteoblast at the fracture line. At 4 W, the bone on both sides of the fracture line was misaligned, resulting in the enlargement of fracture line. A large number of bone marrow cells were

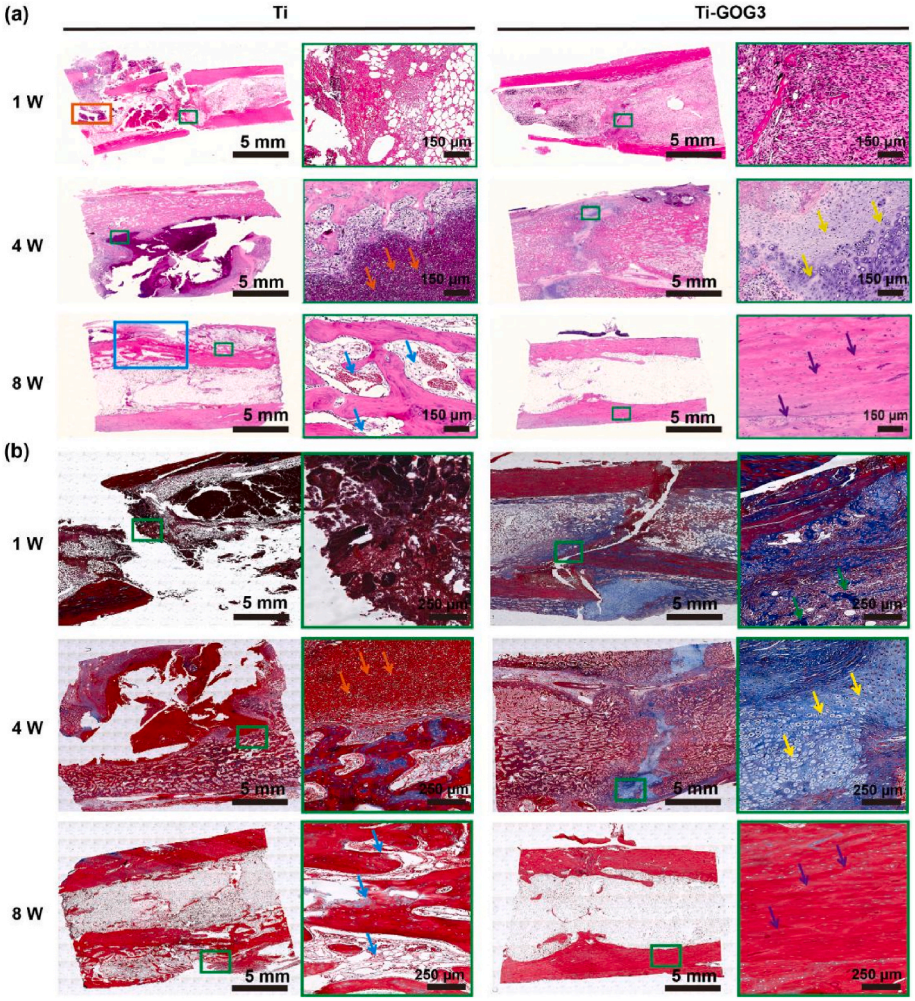

Fig. 8. Histological analysis of the bone tissues. Histological examination by a) H&E and b) Masson's trichrome staining of the bone tissues in the fracture site of Ti and Ti-GOG3 group at 1, 4, and 8 W after surgery (orange arrows, bone marrow cells; yellow arrows, cartilage; red arrows, osteoblasts; blue arrows, low bone density area; purple, high bone density area; orange frame, inflammation-associated cells; blue frame, tibial deformation zone).

observed around the fracture line (marked by orange arrows). The fracture line healed at 8 W, but the cortical bone density was significantly lower than that in the Ti-GOG3 group (marked by blue arrows), demonstrating that the bone recovery was poor. The tibial deformation zone was highlighted by blue frame. The above results showed that infection could reduce the healing speed and quality of fracture, the Ti-GOG3 group could effectively kill bacteria and the group could been beneficial for fracture healing. The Ti group showed severe infection by analyzing the wound healing and blood, which delayed the fracture healing. By self-adaptive antibacterial property, Ti-GOG3 could kill bacteria efficiently to inhibit infection and infection-associated inflammation, which was beneficial for treatment of IAFF. The *in vivo* experiments demonstrated that the Ti-GOG3 could be used for orthopedic implants to treat IAFF.

3. Conclusions

In summary, infection-responsive antibacterial bone plates (Ti-GOG3) with long-term stability were successfully constructed. GS, one of the antibiotics in clinical practice, was successfully conjugated via Schiff base reaction. *In vitro* studies proved that the Ti-GOG3 had long-term stability and infection-responsive antibacterial properties, and favorable biocompatibility. Moreover, Ti-GOG3 could effectively kill bacteria and reduce their colonization on the surface. In an *in vivo* rabbit tibial infected open fracture model, the anti-infection performances of Ti-GOG3 were demonstrated. At early stage, because the Schiff base structure had been broken by the acidic micro-environment produced by bacterial metabolism, Ti-GOG3 showed self-adaptive release profile of GS to eliminate infection. At late stage, because infection and infection-associated inflammation had been inhibited, Ti-GOG3 could promote the formation of new bone, which was beneficial for recovery of bone fracture. The present work provides a facile and universal strategy for the development of various bone implant materials of various shapes with infection-responsive long-term antibacterial properties, which is promising for the treatment of IAFF.

4. Experimental section

The detailed experimental methods were described in Supporting Information.

Declaration of competing interest

The authors declare no conflict of interest.

Data availability

The raw/processed data required to reproduce these findings cannot be shared at this time as the data also forms part of an ongoing study.

Ethics approval and consent to participate

Animal studies were approved by the Ethical Committee of China-Japan Friendship Hospital and conducted according to legal agreement.

CRediT authorship contribution statement

Lujiao Zhang: Methodology, Investigation, Writing – original draft. **Yurun Yang:** Investigation. **Yan-Hua Xiong:** Investigation. **Yu-Qing Zhao:** Investigation. **Zongpeng Xiu:** Investigation. **Hui-Min Ren:** Investigation. **Kai Zhang:** Validation. **Shun Duan:** Conceptualization, Methodology, Supervision, Writing – review & editing, Funding acquisition. **Ying Chen:** Conceptualization, Funding acquisition. **Fu-Jian Xu:** Resources, Supervision, Writing – review & editing, Project administration, Funding acquisition.

Declaration of competing interest

The authors declare that they have no known competing financial interests or personal relationships that could have appeared to influence the work reported in this paper.

Acknowledgements

This work was supported by National Natural Science Foundation of China [Grant Nos. 52122304, 52073024 and 51873012], Beijing Outstanding Young Scientist Program [Grant No. BJJWZYJH01201910010024] and Chinese Association of Rehabilitation Medicine Technology Development Project [Grant No. KFKT-2022-002].

Appendix A. Supplementary data

Supplementary data to this article can be found online at https://doi.org/10.1016/j.bioactmat.2023.01.002.

References

[1] D.G. Murray, Wound infections after surgery for fractured hip: a follow-up study, J. Am. Med. Assoc. 190 (1964) 505–508.
[2] N.J. Hickok, I.M. Shapiro, Immobilized antibiotics to prevent orthopaedic implant infections, Adv. Drug Deliv. Rev. 64 (2012) 1165–1176.
[3] Y. Xie, L. Zhang, Q. Xiong, Y. Gao, W. Ge, P. Tang, Bench-to-bedside strategies for osteoporotic fracture: from osteoimmunology to mechanosensation, Bone Res. 7 (2019) 25–37.
[4] V. Grunwald, B. Eberhardt, A. Bex, A. Florcken, T. Gauler, T. Derlin, M. Panzica, H. R. Durr, K.A. Grotz, R.H. Giles, C. von Falck, A. Graser, A. Muacevic, M. Staehler, An interdisciplinary consensus on the management of bone metastases from renal cell carcinoma, Nat. Rev. Urol. 15 (2018) 511–521.
[5] N.R. Fuggle, E.M. Curtis, K.A. Ward, N.C. Harvey, E.M. Dennison, C. Cooper, Fracture prediction, imaging and screening in osteoporosis, Nat. Rev. Endocrinol. 15 (2019) 535–547.
[6] M.L. Costa, J. Achten, R. Knight, J. Bruce, S.J. Dutton, J. Madan, M. Dritsaki, N. Parsons, M. Fernandez, R. Grant, J. Nanchahal, W.T. Collaborators, Effect of incisional negative pressure wound therapy vs standard wound dressing on deep surgical site infection after surgery for lower limb fractures associated with major trauma: the WHIST randomized clinical trial, J. Am. Med. Assoc. 323 (2020) 519–526.
[7] J.A. Grisso, J.L. Kelsey, B.L. Strom, G.Y. Ghiu, G. Maislin, L.A. O'Brien, S. Hoffman, F. Kaplan, Risk factors for falls as a cause of hip fracture in women, N. Engl. J. Med. 324 (1991) 1326–1331.
[8] C. Wallace, G.E. Reiber, J. LeMaster, D.G. Smith, K. Sullivan, S. Hayes, C. Vath, Incidence of falls, risk factors for falls, and fall-related fractures in individuals with diabetes and a prior foot ulcer, Diabetes Care 25 (2002) 1983–1986.
[9] T.L. Miller, J.D. Harris, C.C. Kaeding, Stress fractures of the ribs and upper extremities: causation, evaluation, and management, Sports Med. 43 (2013) 665–674.
[10] K.L. Margolis, K.E. Ensrud, P.J. Schreiner, H.K. Tabor, Body size and risk for clinical fractures in older women, Ann. Intern. Med. 133 (2000) 123–127.
[11] C.T. Johnson, J.A. Wroe, R. Agarwal, K.E. Martin, R.E. Guldberg, R.M. Donlan, L. F. Westblade, A.J. García, Hydrogel delivery of lysostaphin eliminates orthopedic implant infection by Staphylococcus aureus and supports fracture healing, P. Natl. Acad. Sci. 115 (2018) E4960–E4969.
[12] N. Chik, W.S. Wan Md Zain, A.J. Mohamad, M.Z. Sidek, W.H. Wan Ibrahim, A. Reif, J.H. Rakebrandt, W. Pfleging, X. Liu, Bacterial adhesion on the titanium and stainless-steel surfaces undergone two different treatment methods: polishing and ultrafast laser treatment, IOP Conf. Ser. Mater. Sci. Eng. 358 (2018), 012034.
[13] H. Chouirfa, H. Bouloussa, V. Migonney, C. Falentin-Daudré, Review of titanium surface modification techniques and coatings for antibacterial applications, Acta Biomater. 83 (2019) 37–54.
[14] Z. Jing, R. Ni, J. Wang, X. Lin, D. Fan, Q. Wei, T. Zhang, Y. Zheng, H. Cai, Z. Liu, Practical strategy to construct anti-osteosarcoma bone substitutes by loading cisplatin into 3D-printed titanium alloy implants using a thermosensitive hydrogel, Bioact. Mater. 6 (2021) 4542–4557.
[15] S. Mei, H. Wang, W. Wang, L. Tong, H. Pan, C. Ruan, Q. Ma, M. Liu, H. Yang, L. Zhang, Y. Cheng, Y. Zhang, L. Zhao, P.K. Chu, Antibacterial effects and biocompatibility of titanium surfaces with graded silver incorporation in titania nanotubes, Biomaterials 35 (2014) 4255–4265.
[16] Y. Meng, X. Li, Z. Li, C. Liu, J. Zhao, J. Wang, Y. Liu, X. Yuan, Z. Cui, X. Yang, Surface functionalization of titanium alloy with miR-29b nanocapsules to enhance bone regeneration, ACS Appl. Mater. Interfaces 8 (2016) 5783–5793.
[17] Q. Chen, G.A. Thouas, Metallic implant biomaterials, Mater. Sci. Eng. R 87 (2015) 1–57.
[18] M.H. Elahinia, M. Hashemi, M. Tabesh, S.B. Bhaduri, Manufacturing and processing of NiTi implants: a review, Prog. Mater. Sci. 57 (2012) 911–946.

[19] V. Guarino, F. Causa, P. Taddei, M. di Foggia, G. Ciapetti, D. Martini, C. Fagnano, N. Baldini, L. Ambrosio, Polylactic acid fibre-reinforced polycaprolactone scaffolds for bone tissue engineering, Biomaterials 29 (2008) 3662–3670.
[20] T. Kanno, S. Sukegawa, Y. Furuki, Y. Nariai, J. Sekine, Overview of innovative advances in bioresorbable plate systems for oral and maxillofacial surgery, Jpn Dent. Sci. Rev. 54 (2018) 127–138.
[21] C.R. Arciola, D. Campoccia, L. Montanaro, Implant infections: adhesion, biofilm formation and immune evasion, Nat. Rev. Microbiol. 16 (2018) 397–409.
[22] K. Prasad, O. Bazaka, M. Chua, M. Rochford, L. Fedrick, J. Spoor, R. Symes, M. Tieppo, C. Collins, A. Cao, D. Markwell, K.K. Ostrikov, K. Bazaka, Metallic biomaterials: current challenges and opportunities, Materials 10 (2017) 884–916.
[23] U. Filipovic, R.G. Dahmane, S. Ghannouchi, A. Zore, K. Bohinc, Bacterial adhesion on orthopedic implants, Adv. Colloid Interface Sci. 283 (2020), 102228.
[24] N.G. Daver, S.A. Shelburne, R.L. Atmar, T.P. Giordano, C.E. Stager, C.A. Reitman, A.C. White Jr., Oral step-down therapy is comparable to intravenous therapy for Staphylococcus aureus osteomyelitis, J. Infect. 54 (2007) 539–544.
[25] E.A. Masters, R.P. Trombetta, K.L. de Mesy Bentley, B.F. Boyce, A.L. Gill, S.R. Gill, K. Nishitani, M. Ishikawa, Y. Morita, H. Ito, S.N. Bello-Irizarry, M. Ninomiya, J. D. Brodell Jr., C.C. Lee, S.P. Hao, I. Oh, C. Xie, H.A. Awad, J.L. Daiss, J.R. Owen, S. L. Kates, E.M. Schwarz, G. Muthukrishnan, Evolving concepts in bone infection: redefining "biofilm", "acute vs. chronic osteomyelitis", "the immune proteome" and "local antibiotic therapy, Bone Res. 7 (2019) 20–37.
[26] W. Gao, Y. Chen, Y. Zhang, Q. Zhang, L. Zhang, Nanoparticle-based local antimicrobial drug delivery, Adv. Drug Deliv. Rev. 127 (2018) 46–57.
[27] C.R. Arciola, D. Campoccia, S. Gamberini, M.E. Donati, V. Pirini, L. Visai, P. Speziale, L. Montanaro, Antibiotic resistance in exopolysaccharide-forming Staphylococcus epidermidis clinical isolates from orthopaedic implant infections, Biomaterials 26 (2005) 6530–6535.
[28] J.M.A. Blair, A climate for antibiotic resistance, Nat. Clim. Change 8 (2018) 460–461.
[29] L. Ran, B. Lu, H. Qiu, G. Zhou, J. Jiang, E. Hu, F. Dai, G. Lan, Erythrocyte membrane-camouflaged nanoworms with on-demand antibiotic release for eradicating biofilms using near-infrared irradiation, Bioact. Mater. 6 (2021) 2956–2968.
[30] X. Ge, C. Ren, Y. Ding, G. Chen, X. Lu, K. Wang, F. Ren, M. Yang, Z. Wang, J. Li, X. An, B. Qian, Y. Leng, Micro/nano-structured TiO_2 surface with dual-functional antibacterial effects for biomedical applications, Bioact. Mater. 4 (2019) 346–357.
[31] L.G. Harris, S. Tosatti, M. Wieland, M. Textor, R.G. Richards, Staphylococcus aureus adhesion to titanium oxide surfaces coated with non-functionalized and peptide-functionalized poly(L-lysine)-grafted-poly(ethylene glycol) copolymers, Biomaterials 25 (2004) 4135–4148.
[32] K. Chae, W.Y. Jang, K. Park, J. Lee, H. Kim, K. Lee, C.K. Lee, Y. Lee, S.H. Lee, J. Seo, Antibacterial infection and immune-evasive coating for orthopedic implants, Sci. Adv. 6 (2020), eabb0025.
[33] X. Hu, J. Tian, C. Li, H. Su, R. Qin, Y. Wang, X. Cao, P. Yang, Amyloid-like protein aggregates: a new class of bioinspired materials merging an interfacial anchor with antifouling, Adv. Mater. 32 (2020), 2000128.
[34] Q. Gao, P. Li, H. Zhao, Y. Chen, L. Jiang, P.X. Ma, Methacrylate-ended polypeptides and polypeptoids for antimicrobial and antifouling coatings, Polym. Chem. 8 (2017) 6386–6397.
[35] L. Schnaider, S. Brahmachari, N.W. Schmidt, B. Mensa, S. Shaham-Niv, D. Bychenko, L. Adler-Abramovich, L.J.W. Shimon, S. Kolusheva, W.F. DeGrado, E. Gazit, Self-assembling dipeptide antibacterial nanostructures with membrane disrupting activity, Nat. Commun. 8 (2017) 1365–1374.
[36] X.Y. Zhang, Y.Q. Zhao, Y. Zhang, A. Wang, X. Ding, Y. Li, S. Duan, X. Ding, F.J. Xu, Antimicrobial peptide-conjugated hierarchical antifouling polymer brushes for functionalized catheter surfaces, Biomacromolecules 20 (2019) 4171–4179.
[37] W. Tegge, G. Guerra, A. Höltke, L. Schiller, U. Beutling, K. Harmrolfs, L. Gröbe, H. Wullenkord, C. Xu, H. Weich, M. Brönstrup, Selective bacterial targeting and infection-triggered release of antibiotic colistin conjugates, Angew. Chem. Int. Ed. 60 (2021) 17989–17997.
[38] S. Yu, G. Li, R. Liu, D. Ma, W. Xue, Dendritic Fe_3O_4@Poly(dopamine)@PAMAM nanocomposite as controllable NO-releasing material: a synergistic photothermal and NO antibacterial study, Adv. Funct. Mater. 28 (2018), 1707440.
[39] S. Yu, G. Li, P. Zhao, Q. Cheng, Q. He, D. Ma, W. Xue, NIR-laser-controlled hydrogen-releasing PdH nanohydride for synergistic hydrogen-photothermal antibacterial and wound-healing therapies, Adv. Funct. Mater. 29 (2019), 1905697.
[40] S. Li, S. Dong, W. Xu, S. Tu, L. Yan, C. Zhao, J. Ding, X. Chen, Antibacterial hydrogels, Adv. Sci. 5 (2018), 1700527.
[41] R. Zhang, Y. Liu, M. He, Y. Su, X. Zhao, M. Elimelech, Z. Jiang, Antifouling membranes for sustainable water purification: strategies and mechanisms, Chem. Soc. Rev. 45 (21) (2016) 5888–5924.
[42] A.M.C. Maan, A.H. Hofman, W.M. Vos, M. Kamperman, Recent developments and practical feasibility of polymer-based antifouling coatings, Adv. Funct. Mater. 30 (2020), 2000936.
[43] W. Li, E.S. Thian, M. Wang, Z. Wang, L. Ren, Surface design for antibacterial materials: from fundamentals to advanced strategies, Adv. Sci. 8 (2021), 2100368.
[44] X. Li, H. Bai, Y. Yang, J. Yoon, S. Wang, X. Zhang, Supramolecular antibacterial materials for combatting antibiotic resistance, Adv. Mater. 31 (2019), 1805092.
[45] J. Leng, Y. He, Z. Yuan, B. Tao, K. Li, C. Lin, K. Xu, M. Chen, L. Dai, X. Li, T. J. Huang, K. Cai, Enzymatically-degradable hydrogel coatings on titanium for bacterial infection inhibition and enhanced soft tissue compatibility via a self-adaptive strategy, Bioact. Mater. 6 (2021) 4670–4685.
[46] S. Pu, J. Fu, Y. Liao, L. Ge, Y. Zhou, S. Zhang, S. Zhao, X. Liu, X. Hu, K. Liu, J. Chen, Promoting energy efficiency via a self-adaptive evaporative cooling hydrogel, Adv. Mater. 32 (2020), e1907307.
[47] Y. Kuang, C. Chen, S. He, E.M. Hitz, Y. Wang, W. Gan, R. Mi, L. Hu, A high-performance self-regenerating solar evaporator for continuous water desalination, Adv. Mater. 31 (2019), e1900498.
[48] C. Wang, W. Zhao, B. Cao, Z. Wang, Q. Zhou, S. Lu, L. Lu, M. Zhan, X. Hu, Biofilm-responsive polymeric nanoparticles with self-adaptive deep penetration for in vivo photothermal treatment of implant infection, Chem. Mater. 32 (2020) 7725–7738.
[49] D. Hu, H. Li, B. Wang, Z. Ye, W. Lei, F. Jia, Q. Jin, K.F. Ren, J. Ji, Surface-adaptive gold nanoparticles with effective adherence and enhanced photothermal ablation of methicillin-resistant staphylococcus aureus biofilm, ACS Nano 11 (2017) 9330–9339.
[50] X. Jin, Y.H. Xiong, X.Y. Zhang, R. Wang, Y. Xing, S. Duan, D. Chen, W. Tian, F. J. Xu, Self-adaptive antibacterial porous implants with sustainable responses for infected bone defect therapy, Adv. Funct. Mater. 29 (2019), 1807915.
[51] H.-S. Lee, S.S. Dastgheyb, N.J. Hickok, D.M. Eckmann, R.J. Composto, Targeted release of tobramycin from a pH-responsive grafted bilayer challenged with S. aureus, Biomacromolecules 16 (2015) 650–659.
[52] A. del Campo, C. Echeverría, M. San Martín, R. Cuervo-Rodríguez, M. Fernández-García, A. Muñoz-Bonilla, Porous microstructured surfaces with pH-triggered antibacterial properties, Macromol, Bioscience 19 (2019), 1900127.
[53] B. Wang, H. Liu, Z. Wang, S. Shi, K. Nan, Q. Xu, Z. Ye, H. Chen, A self-defensive antibacterial coating acting through the bacteria-triggered release of a hydrophobic antibiotic from layer-by-layer films, J. Mater. Chem. B 5 (2017) 1498–1506.
[54] S. Yan, H. Shi, L. Song, X. Wang, L. Liu, S. Luan, Y. Yang, J. Yin, Nonleaching bacteria-responsive antibacterial surface based on a unique hierarchical architecture, ACS Appl. Mater. Interfaces 8 (2016) 24471–24481.
[55] L. Yang, C. Wang, L. Li, F. Zhu, X. Ren, Q. Huang, Y. Cheng, Y. Li, Bioinspired integration of naturally occurring molecules towards universal and smart antibacterial coatings, Adv. Funct. Mater. 32 (2022), 2108749.
[56] J. Xu, L. Yang, X. Hu, S. Xu, J. Wang, S. Feng, The effect of polysaccharide types on adsorption properties of LbL assembled multilayer films, Soft Matter 11 (2015) 1794–1799.
[57] H. Zhang, J. Fei, X. Yan, A. Wang, J. Li, Enzyme-responsive release of doxorubicin from monodisperse dipeptide-based nanocarriers for highly efficient cancer treatment in vitro, Adv. Funct. Mater. 25 (2015) 1193–1204.
[58] X. Wei, H. Xiong, D. Zhou, X. Jing, Y. Huang, Ion-assisted fabrication of neutral protein crosslinked sodium alginate nanogels, Carbohydr. Polym. 186 (2018) 45–53.
[59] S. Wu, C. Xu, Y. Zhu, L. Zheng, L. Zhang, Y. Hu, B. Yu, Y. Wang, F.J. Xu, Biofilm-sensitive photodynamic nanoparticles for enhanced penetration and antibacterial efficiency, Adv. Funct. Mater. 31 (2021), 2103591.
[60] Y. Yu, Y. Zhang, Y. Cheng, Y. Wang, Z. Chen, H. Sun, X. Wei, Z. Ma, J. Li, Y. Bai, Z. Wu, X. Zhang, NIR-activated nanosystems with self-modulated bacteria targeting for enhanced biofilm eradication and caries prevention, Bioact. Mater. 13 (2022) 269–285.
[61] P. Merkl, M.-S. Aschtgen, B. Henriques-Normark, G.A. Sotiriou, Biofilm interfacial acidity evaluation by pH-responsive luminescent nanoparticle films, Biosens. Bioelectron. 171 (2021), 112732.
[62] S. Li, M. Pei, T. Wan, H. Yang, S. Gu, Y. Tao, X. Liu, Y. Zhou, W. Xu, P. Xiao, Self-healing hyaluronic acid hydrogels based on dynamic Schiff base linkages as biomaterials, Carbohydr. Polym. 250 (2020), 116922.
[63] D.I. Andersson, N.Q. Balaban, F. Baquero, P. Courvalin, P. Glaser, U. Gophna, R. Kishony, S. Molin, T. Tonjum, Antibiotic resistance: turning evolutionary principles into clinical reality, FEMS Microbiol. Rev. 44 (2020) 171–188.
[64] Z. Zhang, M.M. Jones, C. Sabatini, S.T. Vanyo, M. Yang, A. Kumar, Y. Jiang, M. T. Swihart, M.B. Visser, C. Cheng, Synthesis and antibacterial activity of polymer-antibiotic conjugates incorporated into a resin-based dental adhesive, Biomater. Sci. 9 (2021) 2043–2052.
[65] W. Zimmerli, P. Sendi, Pathogenesis of implant-associated infection: the role of the host, Semin. Immunopathol. 33 (2011) 295–306.
[66] A.D. Gahukamble, A. McDowell, V. Post, J. Salavarrieta Varela, E.T. Rochford, R. G. Richards, S. Patrick, T.F. Moriarty, Propionibacterium acnes and Staphylococcus lugdunensis cause pyogenic osteomyelitis in an intramedullary nail model in rabbits, J. Clin. Microbiol. 52 (2014) 1595–1606.
[67] S. Lee, Y.Y. Chang, J. Lee, S.K. Madhurakkat Perikamana, E.M. Kim, Y.H. Jung, J. H. Yun, H. Shin, Surface engineering of titanium alloy using metal-polyphenol network coating with magnesium ions for improved osseointegration, Biomater. Sci. 8 (2020) 3404–3417.
[68] N. Yokogawa, M. Ishikawa, K. Nishitani, C.A. Beck, H. Tsuchiya, A. Mesfin, S. L. Kates, J.L. Daiss, C. Xie, E.M. Schwarz, Immunotherapy synergizes with debridement and antibiotic therapy in a murine 1-stage exchange model of MRSA implant-associated osteomyelitis, J. Orthop. Res. 36 (2018) 1590–1598.